


Critical behavior of the diffusive susceptible-infected-recovered model

Shengfeng Deng^{*} and Géza Ódor[†]

Institute of Technical Physics and Materials Science, Centre for Energy Research, P.O. Box 49, H-1525 Budapest, Hungary

 (Received 26 August 2022; revised 30 November 2022; accepted 4 January 2023; published 19 January 2023)

The critical behavior of the nondiffusive susceptible-infected-recovered model on lattices had been well established in virtue of its duality symmetry. By performing simulations and scaling analyses for the diffusive variant on the two-dimensional lattice, we show that diffusion for all agents, while rendering this symmetry destroyed, constitutes a singular perturbation that induces asymptotically distinct dynamical and stationary critical behavior from the nondiffusive model. In particular, the manifested crossover behavior in the effective mean-square radius exponents reveals that slow crossover behavior in general diffusive multispecies reaction systems may be ascribed to the interference of multiple length scales and timescales at early times.

DOI: [10.1103/PhysRevE.107.014303](https://doi.org/10.1103/PhysRevE.107.014303)

I. INTRODUCTION

Nonequilibrium systems exhibiting active-to-absorbing phase transitions are fundamentally important for understanding a large variety of natural phenomena [1–6]. Among the relevant models, the susceptible-infected-recovered (SIR) model for the spread of epidemic disease in an ensemble of living beings [7], or the spread of a nonconserved agent in broader contexts (e.g., forest fires [8], chemical reactions [9], and sociology [10]), has long been extensively studied. This model and its numerous variants have been applied to the most varied forms of epidemics [11], and more recently have been attracting a surge of attention due to the COVID-19 pandemic [12,13].

The essence of the model assumes that the individuals can be categorized into susceptible (S), infected (I), and recovered (R) states so that the unidirectional process $S \rightarrow I \rightarrow R$ occurs, upon the assumption that the infected agent can not pop up spontaneously but transmits the disease exclusively upon encounter of $S - I$ pairs ($S + I \xrightarrow{\lambda} 2I$), while infected individuals recover ($I \xrightarrow{\mu} R$) and cannot revert to a susceptible state in any rate. By assuming perfect immunization, the SIR process, which is also often referred to as the *general epidemic process* (GEP) [14], is deeply connected to the bond percolation process both on lattices [14–18] and on networks [19]. Owing to the competition of the two sub-processes, the SIR process manifests a continuous nonequilibrium phase transition that separates the infection dominant regime, where the epidemic spreads infinitely in the thermodynamic limit, and the recovery dominant regime, where the system becomes trapped in an *absorbing state* after some time, characterizing the extinction of the epidemic.

In the past few decades, voluminous numerical simulation [14,20–25] and field-theoretic [16–18] analyses have profoundly established the critical properties of this transition

on d -dimensional lattices to be exactly mapped to the dynamical isotropic percolation (DIP) universality class, except for a subtle difference in their respective local cluster growth probabilities [24]. Moreover, the DIP fixed point remains stable even if partial immunization is implemented, until the model is tuned into the SIS model which belongs to the directed percolation (DP) class [16,20,22,26], or, according to the Harris [27] or Harris-Barghathi-Vojta [28] criteria, if certain quenched spatial disorders or topological disorders are incorporated [29], as long as the transition is not destroyed [30] and the dimensionality is not altered [13].

As a crucial ingredient for mapping to the DIP, all the previous studies tacitly assumed that at least the immune individuals are immobile [31] which in turn enables great simplifications in problem formulation [14,16–18]. However, similar to the pair contact process with diffusion (PCPD) [32] and the diffusive epidemic process (DEP) [33], the effects of diffusion shouldn't be overlooked [13,34], because realistic immune individuals indeed hop around to augment the mixture of the population, so that such model could find wide applications in epidemic spreading among wild grazing and forest animals [35] as well as the spread of human diseases such as whooping cough [36] and COVID-19 (when lockdown measures are imposed to cut out most long-range links and the population is restricted to local mobility), or even in autocatalytic reactions with catalyst degradation [9], to name just a few. Already after taking into account spatial inhomogeneities with the local densities and the diffusion terms for the SIR rate equation

$$\begin{aligned}\partial_t S(x, t) &= D_S \nabla^2 S(x, t) - \lambda S(x, t) I(x, t), \\ \partial_t I(x, t) &= D_I \nabla^2 I(x, t) + \lambda S(x, t) I(x, t) - \mu I(x, t), \\ \partial_t R(x, t) &= D_R \nabla^2 R(x, t) + \mu I(x, t),\end{aligned}\quad (1)$$

it has been shown that the dynamic behavior of such coupled (partial) differential equations depends on the diffusion rates for both systems with homogeneous [36] and inhomogeneous [37] couplings.

^{*} shengfeng.deng@ek-cer.hu

[†] odor@mfa.kfki.hu

What is more, inclusion of diffusion for immune agents may also provoke nontrivial modifications to the critical properties, as remarked by Janssen *et al.* in Ref. [38]. First and foremost, at criticality, the recovered debris left by starting from a single infectious seed build up a fuzzy pattern, in stark contrast to the fully connected percolating cluster in the nondiffusive case (see Fig. 1). More profoundly, from a field-theoretic point of view, after casting “ I ” and “ R ” into the coarse-grained $\mathcal{I}(x, t)$ and $\mathcal{R}(x, t)$ fields [39] in the continuum limit, along with the corresponding response fields $\tilde{\mathcal{I}}(x, t)$ and $\tilde{\mathcal{R}}(x, t)$, the ensuing bosonic field theory action [18] (see the Appendix for the derivation)

$$A = \int d^d x dt \left\{ \underbrace{\tilde{\mathcal{I}} \left[\partial_t - D_I(\tau - \nabla^2) + \frac{g}{2}(2\mathcal{R} - \tilde{\mathcal{I}}) \right]}_{\text{DIP}} \mathcal{I} + \tilde{\mathcal{R}}(\partial_t - D_R \nabla^2) \mathcal{R} - \tilde{\mathcal{R}} \mathcal{I} \right\}, \quad (2)$$

where τ denotes the control parameter, renders the duality symmetry

$$\tilde{\mathcal{I}}(x, t) \leftrightarrow -\mathcal{R}(x, -t) \quad (3)$$

no longer held. Note that the very existence of the DIP transition is induced by the spontaneous breaking of this symmetry [16], which arises only if $D_R = 0$ [16,18] (see Sec. II). Once diffusion for the immune agents sets in, the duality symmetry associated with this local accumulation is lost. The full action then describes a reaction-diffusion-type model involving the active species I and the inert species R : $I + \emptyset \rightarrow 2I$, $I \rightarrow R$, in conjunction with individual diffusion of rates D_I and D_R and reactions for particle number restrictions in a bosonic representation; see Eq. (A1).

While the rate equation system (1) yields qualitatively good predictions for the evolving behavior of an epidemic process, it still amounts to a mean-field treatment in which correlations in the infection interactions had been factorized. Hence, it ignores spatiotemporal fluctuations and correlations of the reaction processes that increasingly become crucial for low-dimensional systems near criticality [1]. To fully account for the effects of fluctuations and correlations when individual diffusion is also present in the SIR model, one can resort either to a field-theoretic analysis [6,16,18], which is usually quite challenging for more complicated models, or to a straightforward implementation of the stochastic reactions via simulations [14,24]. In this work, we will take the latter approach to study the critical properties of the diffusive SIR (DSIR) process on a two-dimensional lattice. Field theory action is primarily introduced to give a more profound motivation for this study. Yet, we hope the numerical results could be beneficial to further advancing field-theoretic analyses as well.

The remainder of this paper is organized as follows: In the next section, we give a detailed exposition on the violation of the duality symmetry in the DSIR. We then detail our simulation method in Sec. III and compute various critical exponents both in the dynamical regime and in the stationary state in Sec. IV. Finally, Sec. V summarizes this work and provides a brief outlook.

II. VIOLATION OF THE DUALITY SYMMETRY

The response field $\tilde{\mathcal{R}}(x, t)$ only appears linearly in the action (2). Hence, it can be integrated out from the path integral to retain only the DIP part of action (2), which is equivalent to computing the functional derivative $\frac{\delta A}{\delta \tilde{\mathcal{R}}} = 0$ [6] that leads to a constraint for the $\mathcal{R}(x, t)$ field

$$\partial_t \mathcal{R} = D_R \nabla^2 \mathcal{R} + \mathcal{I}. \quad (4)$$

Without the presence of diffusion for the immune agents, we simply have

$$\mathcal{I}(x, t) = \partial_t \mathcal{R}(x, t) \text{ and } \mathcal{R}(x, t) = \int_{-\infty}^t dt' \mathcal{I}(x, t'), \quad (5)$$

with which the DIP part of the action (2) can be further manipulated through integrating by parts and becomes [16]

$$\begin{aligned} \mathcal{A}_{\text{DIP}} &= \int d^d x dt \tilde{\mathcal{I}} \left[\partial_t - D_I(\tau - \nabla^2) + \frac{g}{2}(2\mathcal{R} - \tilde{\mathcal{I}}) \right] \partial_t \mathcal{R} \\ &= \int d^d x dt \left\{ \partial_t \mathcal{R} [-\partial_t + D_I(\tau - \nabla^2)] \tilde{\mathcal{I}} - \frac{g}{2} \mathcal{R}^2 \partial_t \tilde{\mathcal{I}} - \frac{g}{2} \tilde{\mathcal{I}}^2 \partial_t \mathcal{R} \right\}. \end{aligned} \quad (6)$$

Now we apply the duality transformation Eq. (3) [$\tilde{\mathcal{I}}(x, t) \leftrightarrow -\mathcal{R}(x, -t) = -\int_{-\infty}^{-t} dt' \mathcal{I}(x, t')$] on \mathcal{A}_{DIP} to substantiate that the DIP action is invariant after transformation:

$$\begin{aligned} \mathcal{A}'_{\text{DIP}} &= \int d^d x dt \left\{ \partial_t [-\tilde{\mathcal{I}}(-t)] [-\partial_t - D_I(\tau - \nabla^2)] \right. \\ &\quad \times [-\mathcal{R}(-t)] - \frac{g}{2} [-\tilde{\mathcal{I}}(-t)]^2 (\partial_t [-\mathcal{R}(-t)]) \\ &\quad \left. - \frac{g}{2} [-\mathcal{R}(-t)]^2 (\partial_t [-\tilde{\mathcal{I}}(-t)]) \right\} \\ &\stackrel{t'=-t}{=} \int d^d x dt' \left\{ \partial_{t'} \mathcal{R}(t') [-\partial_{t'} + D_I(\tau - \nabla^2)] \tilde{\mathcal{I}}(t') \right. \\ &\quad \left. - \frac{g}{2} \tilde{\mathcal{I}}(t')^2 \partial_{t'} \mathcal{R}(t') - \frac{g}{2} \mathcal{R}(t')^2 \partial_{t'} \tilde{\mathcal{I}}(t') \right\} \\ &\stackrel{\text{Eq. (6)}}{=} \mathcal{A}_{\text{DIP}}, \end{aligned} \quad (7)$$

where in the second equation we have again employed integration by parts.

The above derivation demonstrates that, after integrating out the response field $\tilde{\mathcal{R}}$, it is crucial for Eq. (5) to be strictly valid for the DIP part of action (2) to be symmetric under the duality transformation. According to Eq. (4), implementing diffusion for the immune agents immediately spoils this requirement.

III. SIMULATION METHOD

To verify the effects of diffusion on the critical properties, in this paper, we perform large-scale Monte Carlo simulations for the simplest $D_R = D_I = D_S = D$ case on a two-dimensional square lattice, with each site being occupied by exactly one individual. Since individuals constantly jiggle around after the incorporation of diffusion, efficient simulation methods that had been exploited for the nondiffusive SIR

(hereafter referred to as SIR), such as traversing over a linked list for active agents [22], are not feasible in a straightforward way. Henceforth, to reduce the simulation overhead, we resort to the sequential updating scheme [1, 13]. At each Monte Carlo (MC) time step t , it is preferable to implement reactions and individual diffusions into two separate sequential sweeps to prevent diffusion events from interfering with reaction events. The system is then updated as follows.

(1) Two arrays \mathbf{x} and \mathbf{X} (initially, $\mathbf{x} = \mathbf{X}$) of size $N = L \times L$, representing the current and the future states of the system, are maintained to trace the updates. At each site, the state variables x_i and X_i can assume one of the S , I , and R states. During the reaction sweep, depending on the state value X_i of a selected site i , the state is updated either from $X_i = S$ to $X_i = I$ with probability λ if the selected nearest neighbor j for contact is in the state $x_j = I$, or from $X_i = I$ to $X_i = R$ with probability $\mu = 1 - \lambda$; otherwise, X_i remains intact.

(2) In the diffusion sweep, we simply swap the states of a selected site i and its randomly selected neighbor j with respect to identical probability D : $X_i \xrightarrow{D} X_j$. One caveat to note is that the conventional rightward-downward sweep tends to cause a biased diffusion towards the right and the down directions. To counteract this artifact so that individuals diffuse unbiasedly, the lattice is swept alternately in a forward manner for odd time steps, and in a backward manner for even time steps.

(3) Set $\mathbf{x} = \mathbf{X}$ after each cycle of the above two sweeps and increase t by one to start a new updating cycle, until the prescribed/conditioned simulation time is reached.

In principle, the artifact in step 2 can be circumvented with a greater effort by matching the pairs for swapping through a domino tiling [40], permitting a parallel update of the system. Nevertheless, the entirety of the above updates should be considered as happening simultaneously for each time step. As a side remark, note that critical properties of a system are governed by the emerged long-range correlations and are insensitive to microscopic details, as exemplified by the bosonic representation of the DSIR in the Appendix, in which a site can even contain more than one individual. In this respect, any mechanism that provides isotropic *local* mobility of the individuals can be defined as a valid diffusion action, and the above implementation of diffusion for our fully occupied lattice via simple state swapping is justified.

To simulate the critical dynamics of absorbing phase transitions, there are two conventional ways of initializing the runs, i.e., homogeneously filling the lattice with the active agents or starting each run from a single active seed [1]. Due to the irreversible nature of the dynamics, the former only amounts to the relaxational process for recoveries. Therefore, it is customary to study the spreading dynamics by initializing the lattice with a single infectious seed [1, 5, 13, 41] placed at the center of the lattice; cf. the typical clusters obtained at criticality shown in Fig. 1. The growth of clusters is characterized by the number of I individuals $N_I(\lambda, t)$; the survival probability $P_{\text{sur}}(\lambda, t)$ [42], with both quantities averaged over all runs; and the mean-square radius $R_I^2(\lambda, t)$, averaged over survival runs. Simulations were terminated if the distance of any I or R individual away from the center exceeds $L/2$.

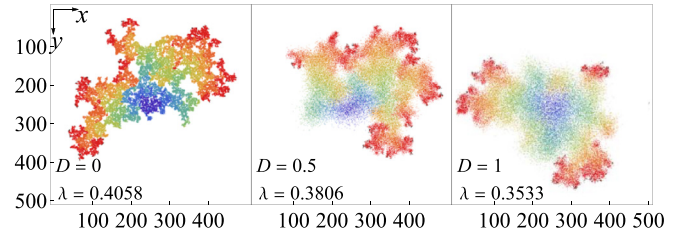


FIG. 1. Snapshots for the critical SIR process with diffusion rates $D = 0, 0.5$, and 1 on a 500×500 lattice. The S and I species are colored in white and black. The rainbow spectrum beared by the R species, from blue to red, linearly marks their relative generating time.

Above the transition point λ_c , after denoting $\Delta = \lambda - \lambda_c$, the following scaling relations hold [5, 18]:

$$N_I(\lambda, t) = t^{\theta_I} \hat{N}_I(\Delta^{\nu_{\parallel}} t), \quad (8a)$$

$$P_{\text{sur}}(\lambda, t) = t^{-\delta} \hat{P}_{\text{sur}}(\Delta^{\nu_{\parallel}} t), \quad (8b)$$

$$R_I^2(\lambda, t) = t^{Z_I} \hat{R}_I^2(\Delta^{\nu_{\parallel}} t), \quad (8c)$$

giving rise to the power laws at criticality,

$$N_I(t) \sim t^{\theta_I}, \quad P_{\text{sur}}(t) \sim t^{-\delta}, \quad R_I^2(t) \sim t^{Z_I}, \quad (9)$$

where θ_I , δ , and $Z_I = 2/z_I = 2\nu/\nu_{\parallel}$ are spreading exponents, whilst ν and ν_{\parallel} are related to the correlation length and the characteristic time, diverging as $\xi \sim \Delta^{-\nu}$ and $t_c \sim \xi^{z_I} \sim \Delta^{-\nu_{\parallel}}$. For two-species systems, it is also appropriate to define the counterparts $N_R(t) \sim t^{\theta_R}$ and $R_R^2(t) \sim t^{Z_R}$, for the R species [43].

IV. CRITICAL EXPONENTS

In this section, we show that after a crossover the dynamical spreading exponents of the DSIR consistently deviate from the SIR/DIP, resulting in an altered hyperscaling relation. In addition, finite-size scaling analyses of the stationary state further corroborate the main conjecture.

As shown in Fig. 2(a), in stark contrast to the SIR, in which a pure power law is manifested for $N_I(t)$ at λ_c , the DSIR process exhibits a crossover before an asymptotic scaling regime is approached. Owing to the competition of diffusive spreading and local reactivity, this crossover can be separated into two stages: first, the initially abundant S content renders the kinetic to be *reaction-limited* and once the established correlations exceed the lattice spacing at $t \sim 10$, the enhanced mixture of S and I populations kicks in a boosted spread; then at large times, the produced R debris effectively dilute the local reactant densities and the system becomes *diffusion-limited* [44]. In finite systems, this process goes on until reachable S individuals are depleted. The observed asymptotic scaling behavior permits one to estimate the transition point λ_c by observing the evolution of the local slope, i.e., the effective exponent

$$\theta_I^{\text{eff}} = \left| \frac{\ln [N_I(t)/N_I(t/b)]}{\ln(b)} \right|, \quad (10)$$

with $b > 1$ [45]; similarly, θ_R^{eff} , δ^{eff} , Z_I^{eff} , and Z_R^{eff} can be defined. The transition point is then identified by spotting the

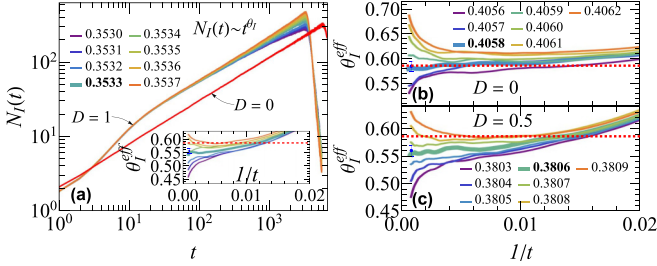


FIG. 2. Growth of the I population $N_I(t)$ from a single infectious seed on a $L = 4001$ square lattice in the vicinity of criticality for (a) $D = 1$, and the evolution of the corresponding effective exponent θ_I^{eff} in the inset, in panel (b) for $D = 0$, and in panel (c) for $D = 0.5$. For comparison, the red solid line in panel (a) depicts the critical $N_I(t)$ result for $D = 0$. The critical points, emphasized by the thick curves, are estimated to $\lambda_c \simeq 0.4058(1)$, $\lambda_c \simeq 0.3806(1)$, and $\lambda_c \simeq 0.3533(1)$ for $D = 0$, $D = 0.5$, and $D = 1$, respectively. The horizontal dashed red line indicates the DIP value; cf. Table I. All results were averaged over 10^4 independent runs.

λ value that gives rise to an asymptotically stationary θ_I^{eff} . Figure 2 illustrates that, on the one hand, the transition point decreases with increasing diffusion rates; on the other hand, while $\theta_I \approx 0.585(10)$ for $D = 0$ conceivably recovers the DIP value, the DSIR exponent value $\theta_I \approx 0.55(2)$ and $0.56(1)$ for $D = 0.5$ and $D = 1$ demonstrate a consistent, albeit slight, deviation from the DIP. This downward shift in θ_I can be understood as a consequence of the above-mentioned dilution effect which mitigates the infections at the infectious front to some extent.

Figure 3 further unambiguously shows departures of other DSIR spreading exponents from those of the SIR, which again align with the DIP. In particular, on top of θ_I^{eff} , which already manifests an evident crossover behavior in the DSIR (cf. Fig. 2), all the remaining effective exponents for DSIR are displaying even more pronounced crossover behaviors as compared to the SIR. Hence, $N_I(t)$ is a more apt observable for critical point estimation, even though it is still quite nontrivial, similarly to the PCPD, to fully take into account the corrections to scalings [32,46], thereby the exponents also seem to exhibit a slight dependence on the implemented diffusion rate [47]; cf. Table I. Yet an important observation to make is that the effective spreading exponents Z_I^{eff} and Z_R^{eff} , while closely clinging to each other since early times for $D = 0$, only close up their noticeable gap and converge to an identical value $Z_I = Z_R = Z$ asymptotically for the DSIR, suggesting that there is really just one unique set of length scale ξ and timescale t_c , that renders a critical system scale invariant.

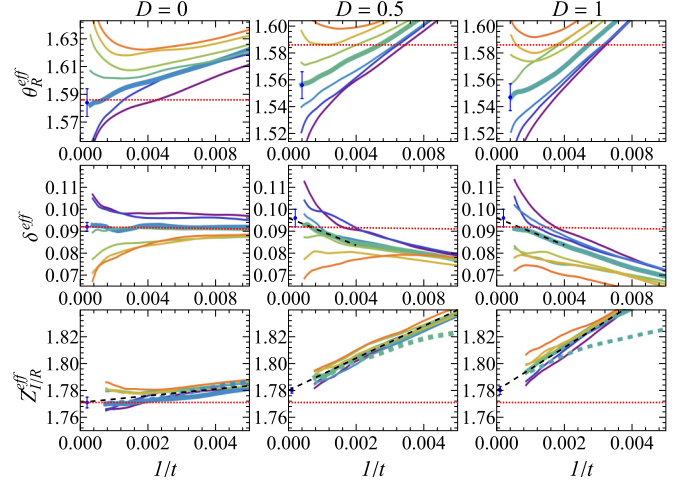


FIG. 3. The effective exponents θ_R^{eff} (top), δ^{eff} (middle), as well as Z_I^{eff} and Z_R^{eff} (bottom) vs $1/t$ for $D = 0, 0.5$, and 1 . The solid thick lines correspond to the respective critical points. In the bottom panels, the dashed thick curves represent the critical Z_R^{eff} , while the dashed black lines extrapolate the effective exponents to $1/t \rightarrow 0$. The standard DIP values are marked by the horizontal dashed red lines; cf. Table I.

Since Z_I^{eff} and Z_R^{eff} are related to the effective correlation exponents, the manifested crossover behavior at early times can then be ascribed to the interference of multiple length and timescales, resulting from diffusion ($\ell_D \sim t^{1/z_D} = t^{1/2}$) and the cutoffs of the correlation functions $\langle \mathcal{I}(r, t) \tilde{\mathcal{I}}(0, 0) \rangle$ and $\langle \mathcal{R}(r, t) \tilde{\mathcal{I}}(0, 0) \rangle$, until the dominant scales ξ and t_c are singled out as $t \rightarrow \infty$, masking processes with shorter characteristic length scales and timescales. Note that $z = 2/Z < z_D = 2$, so the system is superdiffusive and ξ is bound to be larger than ℓ_D .

The DIP spreading exponents are related by the hyperscaling relation [48]

$$\theta_I = \frac{dZ}{2} - 2\delta - 1. \quad (11)$$

Furthermore, the size of the immune cluster should grow linearly with the linear extension of the cluster as $\xi^{d_f} \sim t^{d_f Z/2}$ in a surviving run, where d_f denotes the fractal dimension [8]. By utilizing the hyperscaling relation $d_f = d - \beta/\nu$ and the scaling relation $\delta = \beta/\nu_{\parallel} = \beta Z/2\nu$ [8,18] (see below for the definition of β), the average size of the immune cluster for all runs is then obtained by further multiplying the expression

TABLE I. Critical (and scaling) exponents of the DIP [14,21,25], the SIR ($D = 0$), and the DSIR ($D = 0.5, 1$).^a

D	θ_I	θ_R	δ	Z	ν_{\parallel}	β/ν	γ/ν
DIP	0.586	1.586	0.092	1.771	1.5057	0.1042	1.792
0	0.585(10)	1.584(10)	0.092(2)	1.771(4)	1.51(1)	0.1040(2)	1.810(2)
0.5	0.56(1)	1.55(1)	0.096(4)	1.780(2)	1.46(1)	0.096(2)	1.764(4)
1	0.55(2)	1.54(1)	0.096(4)	1.780(3)	1.47(1)	0.093(3)	1.755(3)

^aUncertainties in the last digit were estimated from the effective exponents for the spreading exponents and from fitting errors for the remaining ones.

with the survival probability

$$N_R(t) \sim t^{dZ/2-2\delta}. \quad (12)$$

Equations (11) and (12) suggest that $\theta_R = \theta_I + 1 \simeq 1.586$ for the DIP. The SIR is naturally in full compliance with these relations.

Now in the DSIR, although the relation $\theta_R \simeq \theta_I + 1$ still seems to be valid, Eq. (12) predicts $\theta_R \approx 1.588(9)$, which is higher than the obtained values 1.55(1) and 1.54(1), implying that the scaling relations $d_f = d - \beta/\nu$ and/or $\delta = \beta/\nu_{\parallel} = \beta Z/2\nu$ utilized for Eq. (12) may not be held for the DSIR. Nonetheless, by taking into account the dilution effect, the density deduced from Eq. (12) should be further reduced by a factor of $t^{-(\theta_{I,\text{DIP}} - \theta_{I,\text{DSIR}})}$, leading

$$\theta_R \simeq \frac{dZ}{2} - 2\delta - (\theta_{I,\text{DIP}} - \theta_{I,\text{DSIR}}) \approx 1.55(2) \quad (13)$$

to be compatible with numerical values within error margins. In addition, the absence of the duality symmetry leads to an apparent violation of the hyperscaling relation Eq. (11) in the DSIR. To break down this discrepancy, we need to take into consideration the renormalization corrections to the naive scaling dimensions, whereupon, when expressed in terms of an arbitrary timescale $T \sim \kappa^{-2/Z}$, we have $[\mathcal{I}] \sim T^{-dZ/4-1/2+\rho}$ and $[\tilde{\mathcal{I}}] \sim T^{-dZ/4+1/2+\chi}$, so that $N_I(t) \sim \langle \int d^d x \mathcal{I}(x, t) \tilde{\mathcal{I}}(0, 0) \rangle \sim t^{\rho+\chi}$ holds, where ρ and χ are the anomalous dimension of the fields. Furthermore, in field theories with absorbing states, one has $[\tilde{\mathcal{I}}] \sim T^{-\delta}$ [48]. Hence, given the symmetry $\tilde{\mathcal{I}}(x, t) \leftrightarrow -\int_{-\infty}^{-t} dt' \mathcal{I}(x, t')$ which renders $\rho = \chi$, Eq. (11) immediately follows in the DIP, whereas in the DSIR, only χ can be eliminated and the hyperscaling relation is altered to

$$\theta_I = \frac{dZ}{4} - \delta - \frac{1}{2} + \rho. \quad (14)$$

Inserting other exponent values, the DSIR value $\rho \approx 0.26(2)$ differs from the DIP value $\rho = \theta_I/2 = 0.293$.

Starting from a seed, the peculiar DSIR dynamical spreading behavior at criticality eventually results in many shattered remnant clusters (cf. Fig. 1), rather than a fully connected percolating cluster as in the DIP/SIR [14,24]. Consequently, the DIP exponents β and γ , associated with the percolation probability $P_{\infty} \sim |\Delta|^{\beta}$ and the mean cluster size $\mathcal{S} \sim |\Delta|^{-\gamma}$, respectively, are not well defined in the DSIR. Nevertheless, in the sense of how one infected seed may affect a sizable population, we can define the ‘‘mean cluster size’’ as the average eventual number of recovered individuals $\mathcal{S} = \langle N_{R\infty} \rangle$ after the disease dies out, then the definitions for the corresponding second moment $\mathcal{M} = \langle N_{R\infty}^2 \rangle$ and the cumulant $U = \mathcal{M}/\mathcal{S}^2$ follow subsequently. Furthermore, for systems with a definite size, the DSIR ‘‘percolation probability’’ P_{∞} can as well be understood as the fraction of runs with any I individuals ever reached the border. Similar to the SIR, these observables are expected to follow the following finite-size scalings at criticality

$$\mathcal{S} \sim L^{\gamma/\nu}, \quad U \sim L^{\beta/\nu}, \quad P_{\infty} \sim L^{-\beta/\nu}, \quad (15)$$

suggesting $UP_{\infty} = \text{const.}$

Figures 4(a) and 4(b) do justify the above finite-size scalings for large system sizes. However, these scalings are

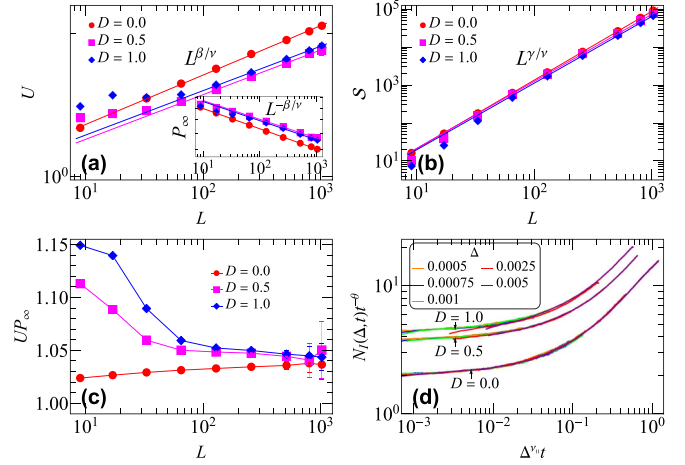


FIG. 4. The finite-size scaling results of (a) U and P_{∞} (inset), (b) \mathcal{S} , and (c) UP_{∞} ; and (d) the data collapse results for $N_I(\Delta, t)$. The results in panels (a)–(c) were averaged from 10^4 to 10^8 runs, and the results in panel (d) were obtained with $L = 2001$, averaged over 10^4 runs.

strongly disturbed by diffusion for smaller system sizes, as evidently shown by the crossover of UP_{∞} in Fig. 4(c). To bridge the dynamical exponents with the stationary scaling exponents, by utilizing Eq. (8a), we also estimated the exponent ν_{\parallel} by collapsing the $N_I(\Delta, t)t^{-\theta_I}$ data, for several Δ s, to the scaling function $\hat{N}_I(\Delta^{\nu_{\parallel}}t)$ with respect to the rescaled time $\Delta^{\nu_{\parallel}}t$. In Fig. 4(d), by fitting all the datasets for different Δ s with an eighth-order polynomial, the best estimations for ν_{\parallel} were obtained by minimizing the sum squared error. Collecting the obtained exponent values in Table I, we see that the DSIR exponents, as well as the deduced exponents $\nu = Z\nu_{\parallel}/2 \approx 1.30(1)$, $\beta \approx 1.21(1)$, and $\gamma \approx 2.29(2)$, again show deviations from those of the DIP/SIR: $\nu \simeq 4/3$, $\beta \simeq 5/36$, and $\gamma \simeq 43/18$ [14]. What is more, since β and γ are not defined on connected clusters, the scaling relations [14,18] $\delta = \beta/\nu_{\parallel} = \beta/\nu \times Z/2$ and $(2\beta + \gamma)/\nu d = 1$ also seem to be violated in the DSIR.

V. SUMMARY

Our simulations and scaling analyses show that the inclusion of diffusion for immune individuals profoundly alters the critical properties of the SIR/DIP in two dimensions. Distinct anomalous scaling dimensions emerge due to the absence of the duality symmetry, leading to an altered hyperscaling relation. In particular, the effective exponents Z_I^{eff} and Z_R^{eff} indicate signatures of multiple length scales and timescales at early times, which qualitatively explain the manifested crossover behavior. Hence, in addition to the PCPD, which may be considered a diffusive coupled two-species system [43] and which also demonstrates a slight exponent change [47], the DSIR provides another example of how diffusion may introduce a singular perturbation, characterized by a slow crossover behavior, to an otherwise well-behaved multispecies system and as in the PCPD [32,43]. Such perturbation may lead to even more intricate dynamics if there are more than one active species. Except for some multispecies directed percolation processes [6,49], the critical properties of general

active-to-absorbing transitions that involve higher-order or multispecies reactions are still scarcely studied and are as yet incompletely understood. We hope our work will shed some light on these fields.

For more realistic epidemiologic modeling, such as in metapopulation models built from internally strongly connected modules [50], structural disorders are strong enough to affect the critical properties. It is then interesting to investigate how critical properties will be affected by diffusion in conjunction with structural disorders, by constructing long-range links [13,51].

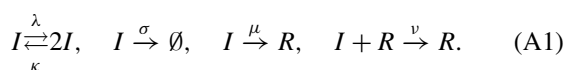
ACKNOWLEDGMENTS

We are very much indebted to Róbert Juhász, Ruslan Mukhamadiarov, and Uwe Täuber for helpful discussions. Support from the Hungarian National Research, Development and Innovation Office NKFIH (K128989) is acknowledged. Most of the numerical work was done on KIFU supercomputers of Hungary.

APPENDIX: FIELD THEORY AND THE ACTION

In this Appendix, we show how Eq. (2) can be obtained by mapping the classical master equation of reaction-diffusion processes onto a field theory action via the Doi-Peliti formalism [52–54] (also see Refs. [6,55,56] for more recent reviews). To begin with, let us note that the action Eq. (2) serves to describe the system near the transition, when the I species is close to extinction so that the density of the I species is vanishingly small as compared to that of the S species. Since S individuals are basically everywhere, it suffices to consider them as a background. Then, similar to the decoupling of predators from preys near the predator extinction transition in the Lotka-Volterra model for predator-prey systems [49], the SIR reactions can be replaced with $I \rightarrow 2I$ and $I \rightarrow R$ by ignoring the existence of the S species. Alternatively and more straightforwardly, for the conventional full-lattice setup [14,24], in which every lattice site is occupied exactly by one individual of S , I or R state, the vast existing S state can be treated as the “vacuum” state \emptyset as in the contact process for the lattice susceptible-infected-susceptible (SIS) model [5,57].

However, as will become clear later, the Doi-Peliti formalism considers particles as “bosonic,” meaning arbitrarily many particles of either species could occupy a lattice point. Therefore, in field theory, to prevent local particle numbers from diverging in the active phase, one can either mimic the mutual exclusion of particles in simulations by imposing a hard-core constraint [58] or more heuristically just add the reaction $I + I \rightarrow I$ and, without loss of generality, the reaction $I \rightarrow \emptyset$, to restrict the local particle numbers [49]. We should remark that retaining either or both of these two reactions will lead to the same effective field theory. Furthermore, the reaction $I + R \rightarrow R$ is added to suppress further productions of R s from I s if an R individual is already present at a location. We then consider the following set of reactions in the bosonic field theory [18]:



Henceforth, we mainly follow the derivations in Sec. 2.2 of Ref. [18], filling necessary gaps. Suppose there is no site occupation number restriction, i.e., we are considering a “bosonic” system with a configuration $\{n, m\} = (\dots, n_i, \dots; \dots, m_i, \dots)$ with n_i particles of species I and m_i particles of species R on site i , etc., where $n_i, m_i = 0, 1, 2, \dots$. The integer occupation number changes of each species (I , R) can be accounted for by using the creation and annihilation operators $\{\hat{a}, \hat{b}\}$ and $\{a, b\}$ that satisfy the *bosonic ladder operator algebra*: $[a_i, a_j] = [\hat{a}_i, \hat{a}_j] = [b_i, b_j] = [\hat{b}_i, \hat{b}_j] = 0$, $[b_i, \hat{b}_j] = [a_i, \hat{a}_j] = \delta_{ij}$. Denoting $|n_i\rangle$ the particle number eigenstate on site i and defining the vacuum state through $a_i|0\rangle = 0$, the bosonic algebra dictates that $a_i|n_i\rangle = n_i|n_i - 1\rangle$, $a_i^\dagger|n_i\rangle = |n_i + 1\rangle$, and $a_i^\dagger a_i|n_i\rangle = n_i|n_i\rangle$. The full state describing a given configuration of the system can then be constructed from the vacuum state as the *Fock product state* $|n, m\rangle = \prod_i \hat{a}_i^{n_i} \hat{b}_i^{m_i} |0\rangle$ and the state of the entire stochastic system $|\Phi(t)\rangle$ is expressed as a superposition of all possible configuration states $|\Phi(t)\rangle = \sum_{\{n,m\}} P(\{n, m\}; t) |\{n, m\}\rangle$, weighted with the time-dependent configuration probability. The master equation for the configuration probability $P(\{n, m\}; t)$ is then cast into an “imaginary-time Schrödinger equation,”

$$\frac{\partial |\Phi(t)\rangle}{\partial t} = -H|\Phi(t)\rangle \Rightarrow |\Phi(t)\rangle = \exp(-Ht)|\Phi(0)\rangle, \quad (\text{A2})$$

where the pseudo-Hamiltonian H is generally not Hermitian.

In terms of the ladder operator language, the gain and the loss terms originating from the master equation for $P(\{n, m\}; t)$ are embedded in H . The rule of thumb is that the losses of particles give rise to the positive loss terms with the number operators $\hat{a}_i a_i$ and $\hat{b}_i b_i$ being raised to the normal-ordered powers of corresponding reactant changes, and the negative terms for the gain balance directly reflect how many particles are destroyed and (re-)created. For example, considering the reaction $kI \xrightarrow{\alpha} lI$ without diffusion, one obtains $H_{\text{react}} = \alpha \sum_i (\hat{a}_i^k - \hat{a}_i^l) a_i^k$. Diffusion between neighboring sites i and j is nothing else but just the reactions $I_i \xrightleftharpoons[D_{j0}]{D_{i0}} I_j$ and $R_i \xrightleftharpoons[D_{R0}]{D_{R0}} R_j$, with the microscopic diffusion rates D_{i0} and D_{R0} . Hence, the reaction scheme (A1), when supplemented with diffusions of both species, yields $H = H_{\text{diff}} + H_{\text{react}}$ with

$$H_{\text{diff}} = \sum_{\langle ij \rangle} [D_{i0}(\hat{a}_i - \hat{a}_j)(a_i - a_j) + D_{R0}(\hat{b}_i - \hat{b}_j)(b_i - b_j)], \quad (\text{A3a})$$

$$H_{\text{react}} = \sum_i [\lambda(1 - \hat{a}_i)\hat{a}_i a_i + \kappa(\hat{a}_i - 1)\hat{a}_i a_i^2 + \sigma(\hat{a}_i - 1)a_i + \mu(\hat{a}_i - \hat{b}_i)a_i + \nu(\hat{a}_i - 1)\hat{b}_i b_i a_i]. \quad (\text{A3b})$$

The field theory action will take its shape within the exponential weight for the statistical average of an arbitrary observable \mathcal{O} . To this end, by introducing the projection state $\langle \mathcal{P} | = \langle 0 | \prod_i e^{a_i + b_i}$, which satisfies $\langle \mathcal{P} | \hat{a}_i = \langle \mathcal{P} | = \langle \mathcal{P} | \hat{b}_i$, the expectation value of \mathcal{O} reads

$$\begin{aligned} \langle \mathcal{O}(t) \rangle &= \sum_{\{n,m\}} \mathcal{O}(\{n, m\}) P(\{n, m\}; t) \\ &= \langle \mathcal{P} | \mathcal{O}(\{\hat{a}a, \hat{b}b\}) | \Phi(t) \rangle \\ &= \langle \mathcal{P} | \mathcal{O}(\{\hat{a}a, \hat{b}b\}) \exp(-Ht) | \Phi(0) \rangle. \end{aligned} \quad (\text{A4})$$

Next, we follow the standard path integral construction [6,55] by splitting the temporal evolution $\exp(-Ht)$ into infinitesimal increments and inserting at each time step the identity operator $\mathbf{1} = \int \prod_i (\frac{d^2\phi}{\pi})(\frac{d^2\varphi}{\pi}) |\{\phi, \varphi\}\rangle \langle\{\phi, \varphi\}|$, where the coherent states $|\phi_i\rangle$ and $|\varphi_i\rangle$ are right eigenstates of the annihilation operators, $a_i|\phi_i\rangle = \phi_i|\phi_i\rangle$ and $b_i|\varphi_i\rangle = \varphi_i|\varphi_i\rangle$, permitting a transformation from q -numbers ($\hat{a}_i, a_i, \hat{b}_i, b_i$) to c -numbers ($\phi_i^*, \phi_i, \varphi_i^*, \varphi_i$). After further taking the continuum limit, $\sum_i \rightarrow h^{-d} \int d^d x$, $\phi_i^* \rightarrow \hat{a}(x, t)$, $\phi_i \rightarrow h^{-d} a(x, t)$, $\varphi_i^* \rightarrow \hat{b}(x, t)$, $\varphi_i \rightarrow h^{-d} b(x, t)$, where h denotes the lattice spacing, the resulting statistical average becomes

$$\langle \mathcal{O}(t) \rangle = \int \mathcal{D}[\hat{a}, \hat{b}, a, b] \mathcal{O}(\{\hat{a}, \hat{b}\}) \exp(-A[\hat{a}, \hat{b}, a, b]), \quad (\text{A5})$$

with the field theory action

$$\begin{aligned} A = & \int d^d x dt [(\hat{a} - 1)\partial_t a + D'_I \nabla \hat{a} \cdot \nabla a \\ & + (\hat{a} - 1)(\sigma - \lambda \hat{a} + \kappa' \hat{a} a) a + (\hat{b} - 1)\partial_t b \\ & + D'_R \nabla \hat{b} \cdot \nabla a + \mu(\hat{a} - \hat{b}) a + \nu'(\hat{a} - 1)\hat{b} b a]. \quad (\text{A6}) \end{aligned}$$

Note that the microscopic diffusion rates have been replaced by the continuum diffusivities $D'_{I/R} = h^2 D_{I0/R0}$, and the rates $\kappa' = h^d \kappa$ and $\nu' = h^d \nu$. In the above expression, the terms $\int d^d x dt \hat{a} \partial_t a$ and $\int d^d x dt \hat{b} \partial_t b$ stemming from the initial and the final factors of the path integral have also been kept. As it is standard, the time limit in the action can be formally taken from $-\infty$ to ∞ .

The fields $\hat{a}(x, t)$, $a(x, t)$, $\hat{b}(x, t)$, and $b(x, t)$ in Eq. (A6) are still complex. To relate them to the density fields $\mathcal{I}(x, t)$ and $\mathcal{R}(x, t)$, one can utilize the fact that $\hat{a}(x, t)a(x, t) = \mathcal{I}(x, t) = \exp(\tilde{\mathcal{I}})\mathcal{I}\exp(-\tilde{\mathcal{I}})$ and $\hat{b}(x, t)b(x, t) = \mathcal{R}(x, t) = \exp(\tilde{\mathcal{R}})\mathcal{R}\exp(-\tilde{\mathcal{R}})$, with the auxiliary (imaginary) response fields $\tilde{\mathcal{I}}(x, t)$ and $\tilde{\mathcal{R}}(x, t)$. Since $a(x, t)$ and $b(x, t)$ carry dimensions of particle densities after performing the continuum limit, we can make the ansatz $\hat{a} = \exp(\tilde{\mathcal{I}})$, $a = \mathcal{I}\exp(-\tilde{\mathcal{I}})$, $\hat{b} = \exp(\tilde{\mathcal{R}})$, and $b = \mathcal{R}\exp(-\tilde{\mathcal{R}})$ to construct a quasi-canonical transformation [18]. Upon employing this transformation, followed by the expansion of the exponentials, integrating by parts, and discarding fourth- and higher-order terms, the action finally takes the following form:

$$\begin{aligned} A = & \int d^d x dt \left\{ \tilde{\mathcal{I}} \partial_t \mathcal{I} - \tilde{\mathcal{I}} \mathcal{I} \partial_t \tilde{\mathcal{I}} - D'_{I1} [\tilde{\mathcal{I}} \nabla^2 \mathcal{I} + \mathcal{I} (\nabla \tilde{\mathcal{I}})^2] + \tilde{\mathcal{I}} \left[(\sigma + \mu - \lambda) + \kappa' \mathcal{I} + \nu' \mathcal{R} - \frac{\lambda + \sigma}{2} \tilde{\mathcal{I}} \right] \mathcal{I} \right. \\ & \left. + \tilde{\mathcal{R}} \partial_t \mathcal{R} - \tilde{\mathcal{R}} \mathcal{R} \partial_t \tilde{\mathcal{R}} - D'_{R1} [\tilde{\mathcal{R}} \nabla^2 \mathcal{R} + \mathcal{R} (\nabla \tilde{\mathcal{R}})^2] - \mu \tilde{\mathcal{R}} \mathcal{I} \right\}. \quad (\text{A7}) \end{aligned}$$

As one rescales the lengths, each term should acquire its respective renormalized (running) coupling constant at different scales. Hence, in the effective field theory, the above expression is rewritten in the following general way:

$$\begin{aligned} A = & \int d^d x dt \left\{ \tilde{\mathcal{I}} \partial_t \mathcal{I} - c \tilde{\mathcal{I}} \mathcal{I} \partial_t \tilde{\mathcal{I}} - D_{I1} \tilde{\mathcal{I}} \nabla^2 \mathcal{I} + D_{I2} \mathcal{I} (\nabla \tilde{\mathcal{I}})^2 + \tau' \tilde{\mathcal{I}} \mathcal{I} + \tilde{\mathcal{I}} [g_1 \mathcal{I} + g_2 \mathcal{R} - g_3 \tilde{\mathcal{I}}] \mathcal{I} \right. \\ & \left. + \tilde{\mathcal{R}} \partial_t \mathcal{R} - c' \tilde{\mathcal{R}} \mathcal{R} \partial_t \tilde{\mathcal{R}} - D_{R1} \tilde{\mathcal{R}} \nabla^2 \mathcal{R} + D_{R2} \mathcal{R} (\nabla \tilde{\mathcal{R}})^2 - g_4 \tilde{\mathcal{R}} \mathcal{I} \right\}. \quad (\text{A8}) \end{aligned}$$

Following the same arguments in Ref. [18], the coupling g_1 turns out to be irrelevant, and the fields as well as the couplings g_2 and g_3 are rescaled by a dimensionful amplitude K as $\tilde{\mathcal{I}} = K^{-1} \tilde{\mathcal{I}}$, $\mathcal{I} = K \mathcal{I}$, $\tilde{\mathcal{R}} = K^{-1} \tilde{\mathcal{R}}$, $\mathcal{R} = K \mathcal{R}$, and $K g_2 = 2K^{-1} g_3 = g'$, leading to

$$\begin{aligned} A = & \int d^d x dt \left\{ \tilde{\mathcal{I}} \partial_t \mathcal{I} - c/K \tilde{\mathcal{I}} \mathcal{I} \partial_t \tilde{\mathcal{I}} - D_{I1} \tilde{\mathcal{I}} \nabla^2 \mathcal{I} + D_{I2}/K \mathcal{I} (\nabla \tilde{\mathcal{I}})^2 + \tau' \tilde{\mathcal{I}} \mathcal{I} + \frac{g'}{2} \tilde{\mathcal{I}} (2\mathcal{R} - \tilde{\mathcal{I}}) \mathcal{I} \right. \\ & \left. + \tilde{\mathcal{R}} \partial_t \mathcal{R} - c'/K \tilde{\mathcal{R}} \mathcal{R} \partial_t \tilde{\mathcal{R}} - D_{R1} \tilde{\mathcal{R}} \nabla^2 \mathcal{R} + D_{R2}/K \mathcal{R} (\nabla \tilde{\mathcal{R}})^2 - g_4 \tilde{\mathcal{R}} \mathcal{I} \right\}, \quad (\text{A9}) \end{aligned}$$

in which, upon rescaling the spatial distances x by a length scale κ^{-1} , the naive scaling dimensions of the fields and couplings are fixed to $[\mathcal{R}]_0 \sim [\tilde{\mathcal{I}}]_0 \sim \kappa^{(d-2)/2}$, $[\mathcal{I}]_0 \sim [\tilde{\mathcal{R}}]_0 \sim \kappa^{(d+2)/2}$, $[\tau]_0 \sim \kappa^2$, $[g]_0 \sim \kappa^{(6-d)/2}$, $[g_4]_0 \sim \kappa^0$, $[c/K]_0 \sim [D_{I2}/K]_0 \sim \kappa^{-(d-2)/2}$, $[c'/K]_0 \sim [D_{R2}/K]_0 \sim \kappa^{-(d+2)/2}$. Consequently, the upper critical dimension $d_c = 6$ remains the same as the DIP, while the couplings c/K , c'/K , D_{I2}/K , and D_{R2}/K are all irrelevant near d_c , rendering

$$A = \int d^d x dt \left\{ \tilde{\mathcal{I}} \partial_t \mathcal{I} - D_{I1} \tilde{\mathcal{I}} \nabla^2 \mathcal{I} + \tau' \tilde{\mathcal{I}} \mathcal{I} + \frac{g'}{2} \tilde{\mathcal{I}} (2\mathcal{R} - \tilde{\mathcal{I}}) \mathcal{I} + \tilde{\mathcal{R}} \partial_t \mathcal{R} - D_{R1} \tilde{\mathcal{R}} \nabla^2 \mathcal{R} - g_4 \tilde{\mathcal{R}} \mathcal{I} \right\}. \quad (\text{A10})$$

Finally, we note that g_4 is naively dimensionless and what is more, there are no diagrams to renormalize it, implying that it will remain dimensionless with respect to rescaling. Hence, it is customary to rescale the time $t \rightarrow t' = g_4 t$ to eliminate g_4 . Upon renaming the couplings to $D_I = D_{I1}/g_4$, $D_R = D_{R1}/g_4$, $D\tau = \tau'/g_4$, and $g = g'/g_4$, we arrive at the action (2).

- [1] H. Hinrichsen, Nonequilibrium critical phenomena and phase transitions into absorbing states, *Adv. Phys.* **49**, 815 (2000).
- [2] G. Ódor, Universality classes in nonequilibrium lattice systems, *Rev. Mod. Phys.* **76**, 663 (2004).
- [3] J. Marro and R. Dickman, *Nonequilibrium Phase Transitions in Lattice Models* (Cambridge University Press, Cambridge, UK, 2005).
- [4] G. Ódor, *Universality in Nonequilibrium Lattice Systems: Theoretical Foundations* (World Scientific, Singapore, 2008).
- [5] M. Henkel, H. Hinrichsen, S. Lübeck, and M. Pleimling, *Nonequilibrium Phase Transitions*, Vol. 1 (Springer, Berlin, 2008).
- [6] U. C. Täuber, *Critical dynamics: A Field Theory Approach to Equilibrium and Nonequilibrium Scaling Behavior* (Cambridge University Press, Cambridge, UK, 2014).
- [7] W. O. Kermack and A. G. McKendrick, A contribution to the mathematical theory of epidemics, *Proc. R. Soc. A: Math. Phys. Eng. Sci.* **115**, 700 (1927); N. T. J. Bailey, *The Mathematical Theory of Infectious Diseases and Its Applications*, 2nd ed. (Griffin, London, 1975), pp. 413–413; J. D. Murray, *Mathematical Biology I. An Introduction* (Springer, Berlin, 2002); R. M. Anderson, *The Population Dynamics of Infectious Diseases: Theory and Applications* Springer Science+Business Media, Dordrecht, 1982; R. Pastor-Satorras, C. Castellano, P. Van Mieghem, and A. Vespignani, Epidemic processes in complex networks, *Rev. Mod. Phys.* **87**, 925 (2015).
- [8] D. Stauffer and A. Aharony, *Introduction to Percolation Theory* (Taylor & Francis, Oxford, UK, 2018).
- [9] C. M. Simon, The SIR dynamic model of infectious disease transmission and its analogy with chemical kinetics, *PeerJ Phys. Chem.* **2**, e14 (2020).
- [10] L. Zhao, H. Cui, X. Qiu, X. Wang, and J. Wang, SIR rumor spreading model in the new media age, *Physica A* **392**, 995 (2013).
- [11] M. Amaku, F. A. B. Coutinho, R. S. Azevedo, M. N. Burattini, L. F. Lopez, and E. Massad, Vaccination against rubella: Analysis of the temporal evolution of the age-dependent force of infection and the effects of different contact patterns, *Phys. Rev. E* **67**, 051907 (2003); D. M. Hartley, J. G. Morris Jr, and D. L. Smith, Hyperinfectivity: A critical element in the ability of *V. cholerae* to cause epidemics? *PLoS Med.* **3**, e7 (2006); L. Zou, W. Zhang, and S. Ruan, Modeling the transmission dynamics and control of hepatitis b virus in China, *J. Theor. Biol.* **262**, 330 (2010); D. Kühnert, T. Stadler, T. G. Vaughan, and A. J. Drummond, Simultaneous reconstruction of evolutionary history and epidemiological dynamics from viral sequences with the birth–death SIR model, *J. R. Soc. Interface* **11**, 20131106 (2014); Y. Kim, A. V. Barber, and S. Lee, Modeling influenza transmission dynamics with media coverage data of the 2009 H1N1 outbreak in Korea, *PLoS One* **15**, e0232580 (2020).
- [12] G. C. Calafiore, C. Novara, and C. Possieri, A modified SIR model for the COVID-19 contagion in Italy, *Proceedings of the 2020 59th IEEE Conference on Decision and Control (CDC)* (IEEE, 2020), pp. 3889–3894; P. G. Walker, C. Whittaker, O. J. Watson, M. Baguelin, P. Winskill, A. Hamlet, B. A. Djafaara, Z. Cucunubá, D. Olivera Mesa, W. Green *et al.*, The impact of COVID-19 and strategies for mitigation and suppression in low-and middle-income countries, *Science* **369**, 413 (2020); R. I. Mukhamadiarov, S. Deng, S. R. Serrao, R. Nandi, L. H. Yao, U. C. Täuber *et al.*, Social distancing and epidemic resurgence in agent-based susceptible-infectious-recovered models, *Sci. Rep.* **11**, 130 (2021).
- [13] G. Ódor, Nonuniversal power-law dynamics of susceptible-infected-recovered models on hierarchical modular networks, *Phys. Rev. E* **103**, 062112 (2021); Erratum: Nonuniversal power-law dynamics of susceptible-infected-recovered models on hierarchical modular networks [Phys. Rev. E 103, 062112 (2021)], **106**, 029901(E) (2022).
- [14] P. Grassberger, On the critical behavior of the general epidemic process and dynamical percolation, *Math. Biosci.* **63**, 157 (1983).
- [15] K. Kuulasmaa and S. Zachary, On spatial general epidemics and bond percolation processes, *J. Appl. Probab.* **21**, 911 (1984).
- [16] H. K. Janssen, Renormalized field theory of dynamical percolation, *Z. Phys. B* **58**, 311 (1985).
- [17] J. L. Cardy and P. Grassberger, Epidemic models and percolation, *J. Phys. A Math. Theor.* **18**, L267 (1985).
- [18] H.-K. Janssen and U. C. Täuber, The field theory approach to percolation processes, *Ann. Phys.* **315**, 147 (2005).
- [19] C. Moore and M. E. J. Newman, Epidemics and percolation in small-world networks, *Phys. Rev. E* **61**, 5678 (2000); M. E. J. Newman, I. Jensen, and R. M. Ziff, Percolation and epidemics in a two-dimensional small world, *ibid.* **65**, 021904 (2002); M. E. J. Newman, Spread of epidemic disease on networks, *ibid.* **66**, 016128 (2002); L. Sander, C. Warren, I. Sokolov, C. Simon, and J. Koopman, Percolation on heterogeneous networks as a model for epidemics, *Math. Biosci.* **180**, 293 (2002); E. Kenah and J. M. Robins, Second look at the spread of epidemics on networks, *Phys. Rev. E* **76**, 036113 (2007).
- [20] P. Grassberger, H. Chaté, and G. Rousseau, Spreading in media with long-time memory, *Phys. Rev. E* **55**, 2488 (1997).
- [21] M. A. Munoz, R. Dickman, A. Vespignani, and S. Zapperi, Avalanche and spreading exponents in systems with absorbing states, *Phys. Rev. E* **59**, 6175 (1999).
- [22] S. M. Dammer and H. Hinrichsen, Spreading with immunization in high dimensions, *J. Stat. Mech.: Theor. Exp.* (2004) P07011.
- [23] D. R. De Souza and T. Tomé, Stochastic lattice gas model describing the dynamics of the SIRS epidemic process, *Physica A* **389**, 1142 (2010).
- [24] T. Tomé and R. M. Ziff, Critical behavior of the susceptible-infected-recovered model on a square lattice, *Phys. Rev. E* **82**, 051921 (2010).
- [25] D. R. De Souza, T. Tomé, and R. M. Ziff, A new scale-invariant ratio and finite-size scaling for the stochastic susceptible–infected–recovered model, *J. Stat. Mech. Theory Exp.* (2011) P03006.
- [26] A. Jiménez-Dalmaroni and H. Hinrichsen, Epidemic processes with immunization, *Phys. Rev. E* **68**, 036103 (2003).
- [27] A. B. Harris, Effect of random defects on the critical behaviour of Ising models, *J. Phys. C: Solid State Phys.* **7**, 1671 (1974).
- [28] H. Barghathi and T. Vojta, Phase transitions on random lattices: How random is topological disorder?, *Phys. Rev. Lett.* **113**, 120602 (2014); M. Schrauth, J. S. E. Portela, and F. Goth, Violation of the Harris-Barghathi-Vojta criterion, *ibid.* **121**, 100601 (2018).
- [29] G. Santos, T. Alves, G. Alves, A. Macedo-Filho, and R. Ferreira, Epidemic outbreaks on two-dimensional quasiperiodic

- lattices, *Phys. Lett. A* **384**, 126063 (2020); C. H. A. Ferraz, A nonabsorbing SIR stochastic lattice gas model on hybrid lattices, *ibid.* **424**, 127871 (2022); R. I. Mukhamadiarov and U. C. Täuber, Effects of lattice dilution on the nonequilibrium phase transition in the stochastic susceptible-infectious-recovered model, *Phys. Rev. E* **106**, 034132 (2022).
- [30] L. Sander, C. Warren, and I. Sokolov, Epidemics, disorder, and percolation, *Physica A* **325**, 1 (2003).
- [31] Most previous studies assumed all individuals are immobile, permitting faster simulation methods. The spread of the epidemic gives rise to an “effective diffusion” for the infected species [18].
- [32] G. Ódor, Critical behavior of the one-dimensional annihilation-fission process $2A \rightarrow \emptyset$, $2A \rightarrow 3A$, *Phys. Rev. E* **62**, R3027 (2000); Phase transition of the one-dimensional coagulation-production process, *ibid.* **63**, 067104 (2001); Critical behavior of the one-dimensional diffusive pair contact process, *ibid.* **67**, 016111 (2003); M. Henkel and H. Hinrichsen, The nonequilibrium phase transition of the pair-contact process with diffusion, *J. Phys. A Math. Theor.* **37**, R117 (2004).
- [33] B. Polovnikov, P. Wilke, and E. Frey, Subdiffusive Activity Spreading in the Diffusive Epidemic Process, *Phys. Rev. Lett.* **128**, 078302 (2022).
- [34] A. Okubo and S. A. Levin, *Diffusion and Ecological Problems: Modern Perspectives*, Vol. 14 (Springer, Berlin, 2001).
- [35] A. M. Fofana and A. Hurford, Mechanistic movement models to understand epidemic spread, *Philos. Trans. R. Soc. B: Biol. Sci.* **372**, 20160086 (2017).
- [36] S. Chinviriyasit and W. Chinviriyasit, Numerical modelling of an SIR epidemic model with diffusion, *Appl. Math. Comput.* **216**, 395 (2010).
- [37] H. Sakaguchi and Y. Nakao, Slow decay of infection in the inhomogeneous susceptible-infected-recovered model, *Phys. Rev. E* **103**, 012301 (2021).
- [38] H.-K. Janssen, M. Müller, and O. Stenull, Generalized epidemic process and tricritical dynamic percolation, *Phys. Rev. E* **70**, 026114 (2004).
- [39] The local densities in Eq. (1) are measured for a particular mesoscopic scale, while the fields in Eq. (2) can be arbitrarily rescaled in the continuum limit and can carry anomalous dimensions.
- [40] R. Kenyon, Lectures on dimers, [arXiv:0910.3129](https://arxiv.org/abs/0910.3129).
- [41] P. Grassberger and A. de la Torre, Reggeon field theory (Schlögl’s first model) on a lattice: Monte Carlo calculations of critical behavior, *Ann. Phys.* **122**, 373 (1979).
- [42] A run up to time t is surviving provided $N_I(t) > 0$.
- [43] S. Deng, W. Li, and U. C. Täuber, Coupled two-species model for the pair contact process with diffusion, *Phys. Rev. E* **102**, 042126 (2020).
- [44] The dilution of local reactant densities by R individuals would be noticeable only at the critical point though, as for $\lambda > \lambda_c$ one would have a circular infectious front, which will be always ahead of R individuals.
- [45] We used $b = 1.4$ and employed moving average to smooth out local fluctuations.
- [46] S.-C. Park, Critical decay exponent of the pair contact process with diffusion, *Phys. Rev. E* **90**, 052115 (2014).
- [47] Although the DSIR exponents only slightly deviate from the DIP values, note that the most precise decay exponent of the PCPD also differs from that of the pair contact process (PCP, i.e., DP) by just ~ 0.014 [46]. Since the R species is inert, we speculate that the DSIR is less affected by corrections to scaling as compared to the PCPD, as suggested by the asymptotically identical values of Z_l^{eff} and Z_R^{eff} ; also cf. Fig. 5 of Ref. [43]. Reference [29] studied a similar DSIR process with a critical population density and with a relatively smaller system size; it seems these slight deviations were not captured due to their larger error margins.
- [48] M. A. Munoz, G. Grinstein, and Y. Tu, Survival probability and field theory in systems with absorbing states, *Phys. Rev. E* **56**, 5101 (1997).
- [49] H. K. Janssen, Spontaneous Symmetry Breaking in Directed Percolation with Many Colors: Differentiation of species in the Gribov Process, *Phys. Rev. Lett.* **78**, 2890 (1997); U. C. Täuber, M. J. Howard, and H. Hinrichsen, Multicritical behavior in coupled directed percolation processes, *ibid.* **80**, 2165 (1998); U. C. Täuber, Population oscillations in spatial stochastic Lotka–Volterra models: A field-theoretic perturbational analysis, *J. Phys. A: Math. Theor.* **45**, 405002 (2012).
- [50] V. Colizza and A. Vespignani, Epidemic modeling in metapopulation systems with heterogeneous coupling pattern: Theory and simulations, *J. Theor. Biol.* **251**, 450 (2008).
- [51] R. I. Mukhamadiarov, S. Deng, S. R. Serrao, L. M. Childs, U. C. Täuber *et al.*, Requirements for the containment of COVID-19 disease outbreaks through periodic testing, isolation, and quarantine, *J. Phys. A: Math. Theor.* **55**, 034001 (2022).
- [52] M. Doi, Second quantization representation for classical many-particle system, *J. Phys. A: Math. Gen.* **9**, 1465 (1976).
- [53] M. Doi, Stochastic theory of diffusion-controlled reaction, *J. Phys. A: Math. Gen.* **9**, 1479 (1976).
- [54] L. Peliti, Path integral approach to birth-death processes on a lattice, *J. Phys. France* **46**, 1469 (1985).
- [55] U. C. Täuber, M. Howard, and B. P. Vollmayr-Lee, Applications of field-theoretic renormalization group methods to reaction–diffusion problems, *J. Phys. A: Math. Gen.* **38**, R79 (2005).
- [56] J. Cardy, G. Falkovich, and K. Gawędzki, *Non-equilibrium Statistical Mechanics and Turbulence*, Vol. 355 (Cambridge University Press, Cambridge, UK, 2008).
- [57] T. E. Harris, Contact interactions on a lattice, *Ann. Probab.* **2**, 969 (1974).
- [58] F. van Wijland, Field theory for reaction-diffusion processes with hard-core particles, *Phys. Rev. E* **63**, 022101 (2001).